Received: 26 June 2020 | Revised: 15 August 2020 | Accepted: 20 August 2020

DOI: 10.1002/ardp.202000214

FULL PAPER

DPhG ARCH PHARM Archiv der Pharmazie

Synthesis of new arylazopyrazoles as apoptosis inducers: Candidates to inhibit proliferation of MCF-7 cells

Magda M. F. Ismail | Dalia H. Soliman | Rehab Sabour | Amel M. Farrag

Department of Pharmaceutical Chemistry, Faculty of Pharmacy (Girls), Al-Azhar University, Cairo, Egypt

Correspondence
Amel M. Farrag, Department of Pharmaceutical Chemistry, Faculty of Pharmacy, Al-Azhar University, Nasr City, Cairo 11754, Egypt.
Email: amelfarrag@ymail.com

Abstract

New 4-arylazo-3,5-diamino-1*H*-pyrazole derivatives substituted in the 4-aryl ring with the acetyl moiety were designed and synthesized . The antiproliferative activity of the novel arylazopyrazoles was examined against the MCF-7 cell line. Among all target compounds, **8b** (IC_{50} 3.0 μM) and **8f** (IC_{50} 4.0 μM) displayed higher cytotoxicity as compared with the reference standard imatinib (IC_{50} 7.0 μM). Further studies to explore the mechanism of action were performed on the most active hit of our library, **8b**, via anti-CDK2 kinase activity. It demonstrated good inhibitory effects for CDK2 (IC_{50} 0.24 μM) with 62.5% inhibition, compared with imatinib. The cell cycle analysis in the MCF-7 cell line revealed apoptosis induction by **8b** and cell cycle arrest at the S phase. Docking in the CDK2 active site and pharmacophore modeling confirmed the affinity of **8b** to the CDK2 active site. Absorption, distribution, metabolism, and excretion studies revealed that our target compounds are orally bioavailable, with no permeation through the blood–brain barrier.

KEYWORDS

antiproliferative agents, breast cancer cells, MCF-7, pyrazole, synthesis

1 | INTRODUCTION

Cancer is appraised among the prominent causes of ailment and deaths across the board.[1,2] Breast cancer is one of the pronounced widespread cancers in females and the next most common reason for malignancy-related mortality. It has also obtruded to be one of the most common cancers in 2016, amidst other cancers.[I,4] In the face of the advances in the treatment of solid tumors (e.g., breast and ovarian cancers), the survival rates are stock-still markedly low.[5] This emphasizes the urgent need to develop effective and more selective chemotherapeutic agents. Cancer is usually figured to be a disease of the cell cycle. Intrinsically, it is not astonishing that the cell cycle deregulation is one of the most prevalent alterations during tumor progression. Progression of the cell cycle is a well-ordered and strongly controlled process that includes diverse checkpoints that assess cell size, extracellular growth signals, and DNA integrity.[5]

Pyrazole derivatives play an influential role among antitumor agents.[6] These compounds have been validated to be useful candidates due to their strong inhibitory activities against $BRAF^{V600E}$, EGFR, CDK2, telomerase, ROS receptor tyrosine kinase, and Aurora-A kinase. The most important role of aryl pyrazoles is as an antitumor agent, with two drugs being available in the market, ruxolitinib (Jakavi®); 3-[4-(7*H*-pyrrolo[2,3-*d*]pyrimidin-4-yl)-1*H*-pyrazol-1-yl]-3-cyclopentylpropanenitrile)[7] and crizotinib (XALKORI®; 3-[(1*R*)-1-(2,6-dichloro-3-fluorophenyl)ethoxy]-5-[1-(4-piperidinyl)-1*H*-pyrazol-4-yl]-2-pyridinamine).[8] Kryštof et al.[9] investigated big series of arylazopyrazoles, the most potent inhibitor, 4-[(3,5-diamino-1*H*-pyrazol-4-yl)diazenyl]phenol (lead compound, CAN508), and revealed that it reduced the frequency of the S phase cell line HT-29 in antiproliferation assays. Depending on CAN508 results, many anticancer arylazopyrazoles were synthesized via a molecular modification to improve cytotoxicity, CDK activity, and their antiproliferative potential against the MCF-7 cancer cell line.[10,11]

On the basis of the literature and as an extension to our search about new therapy to breast adenocarcinoma,[12] the synthesis of a new series of 4-arylazo-3,5-diamino-1*H*-pyrazole bearing 4-acetyl function on the aryl moiety, developed from CAN508, was interesting. Some optimization strategies will be followed, namely, *bioisosteric*

replacement, *chain extension*, and *variation of substituents*, to explore the effects of these structural modifications on the cytotoxic activity (Figure 1). The antiproliferative activity of these candidates will be evaluated against the MCF-7 breast cancer cell line. Additionally, a study of the inhibitory activity on CDK2 and cell cycle analysis will be conducted for the most active compound. Finally, molecular docking on the active site of CDK2 and three-dimensional (3D) pharmacophore model of the most active hit will be performed to investigate the structural characteristics managing the antiproliferative activities.

2 | RESULTS AND DISCUSSION

2.1 | Chemistry

The route adopted for the synthesis of new pyrazole derivatives is illustrated in Schemes 1 and 2. The diazonium salt of *p*-aminoacetophenone was coupled with malononitrile[13–15] in ethanol in the presence of sodium acetate. The resulting coupled product was formulated as 2-[(4-acetylphenyl)diazenyl]malononitrile **2**. Aminopyrazoles **3a,b** were obtained by refluxing **2** with hydrazine hydrate in ethanol,[15,16] whereas **3c** was obtained by using phenylhydrazine in glacial acetic acid.[14] Regarding the synthesis of compounds **4**, when the diazonium salt of compound **3a** was coupled with 3-phenyl-1*H*-pyrazol-5(4*H*)-one,[17] the corresponding arylazo derivative **4a** was afforded. Similarly, the diazonium salt of **3b** was coupled with β-naphthol to yield the arylazo derivative **4b** in a good yield.

However, bioisosteric replacement of 3,5-diamino substituents with 3,5-dimethyl groups, as in arylazopyrazoles **6a,b**, was attempted. First, the intermediate 3-[2-(4-acetylphenyl)hydrazono]pentane-2,4-dione (**5**)[18] was prepared by the reaction of *p*-aminoacetophenone with acetyl acetone in the presence of sodium nitrite and sodium acetate. Then, the target compounds 1-{4-[(3,5-dimethyl-1*H*-pyrazol-4-yl)diazenyl]phenyl}ethanone (**6a**) and 1-{4-[(3,5-dimethyl-1-phenyl-1*H*-pyrazol-4-yl)diazenyl]phenyl}ethanone (**6b**) were prepared by cyclocondensation reaction of the intermediate **5** (0.01 mol) with hydrazine hydrate and phenylhydrazine, respectively, in acetic acid (Scheme 1).

Acylation of the 5-amino functionality of **3a,b** produced the corresponding *N*-acylated products, **7a,b.** Acylation proceeded via stirring of **3a,b** with 2,4-dichlorobenzoyl chloride or benzoyl chloride in DMF for 4 hr.[19] Moreover, the synthesis of a series of Schiff's bases **8a–h** was achieved through the reaction with various substituted aromatic aldehydes or acetophenones in ethanol,[20] in the presence of a basic medium (fused AcONa; Scheme 2).

2.2 | Antitumor studies

2.2.1 | In vitro antitumor activity against human breast cancer cells (MCF-7)

The in vitro antitumor activity against human breast cancer cells (MCF-7) of the 17 target compounds was assessed in the cell culture lab, College of Pharmacy, Al-Azhar University, Cairo, Egypt. Imatinib and CAN508 were used, which showed IC_{50} values of 6.00 and 62.00 μM. The cytotoxicity of the target compounds on the MCF-7 profile clarified variable activities, compared with imatinib and CAN508, as presented in Table 1.

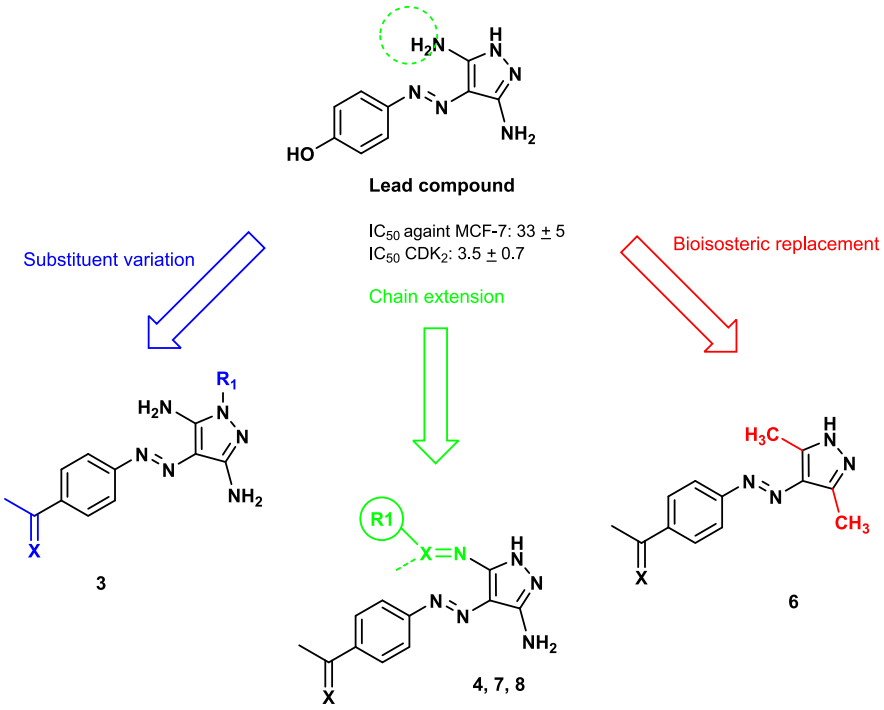

FIGURE 1 The design of the target compounds

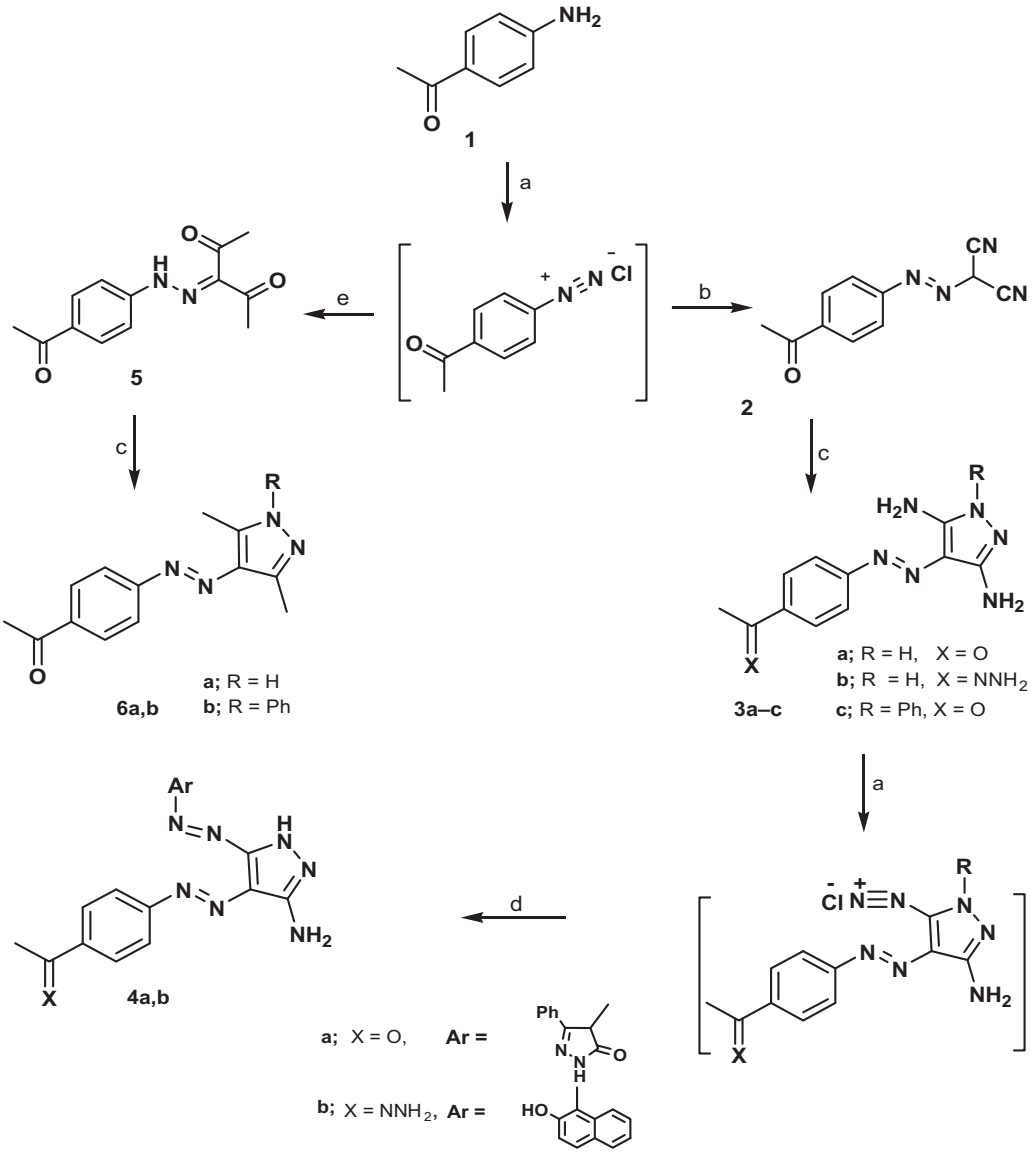

SCHEME 1 The synthesis of compounds **6a,b** and **4a,b**. Reagents and conditions: (a) $NaNO_2$/HCl/0°C, stirring; (b) $CH_2(CN)_2$/NaOAc/EtOH, stirring 30 min/cooling; (c) $RNHNH_2$/EtOH, reflux, 4 hr; (d) 3-phenyl-1*H*-pyrazol-5(4*H*)-one or β-naphthol/sodium acetate/EtOH, stirring 30 min/cooling; (e) acetylacetone/NaOAc/EtOH, stirring 30 min/cooling

Noticeably, most of the target compounds bearing 4-acetyl functionality on the aryl moiety (**3a**, **4a**, **6b**, **7a**, **8b**, and **8f**) showed a potent to moderate antiproliferative activity against the MCF-7 cell line (IC_{50} 3.08–38.7 μM; Figure 2), whereas most of their counterparts carrying the 4-hydrazonoethyl group lacked activity. Thus, the *variation of substituent* has a crucial role in cytotoxicity. In diamino arylazopyrazole **3a** (IC_{50} = 26.86 μM), when NH of pyrazole is substituted with the phenyl moiety (N-Ph), as in **3c** (IC_{50} = > 100 μM), the activity is significantly reduced, which means that the NH group of pyrazole is detrimental for the activity. On the contrary, compound **6** where *bioisosteric replacement* occurs in 3,5-dimethyl instead of 3,5-diamino of the lead compound, it is interesting to note that **6b** (R_1 = –N(Ph)–) showed moderate cytotoxicity (IC_{50} = 38.7 μM), whereas **6a** (R_1 = –NH–) was inactive. This means that the lipophilic criterion in this type of compound may be necessary.

Regarding *extension at **p-5*** via adding an extra arylazo group, a moderate anticancer activity (IC_{50} = 34.7 μM) was noticed for the coupling product **4a** , which bears pyrazolinyl-azo moiety, whereas substituent variation (2-naphthol-1-yl) in **4b** abolished the activity. Other compounds underwent an *extension* tactic via acylation of 5-amino group such as acylation of **3a** with 2,4-dichlorobenzoyl chloride to yield **7a** with a good anticancer activity (IC_{50} = 13.8 μM); however, *N*-benzoylated derivative, **7b**, displayed a weak activity against the MCF-7 cell line. As a continuation for the synthesis of new analogs with *chain extension* at 5-amino of pyrazole, Schiff bases **8a–h** were furnished through a reaction with various aldehydes or ketones. It was clear that **8b** (IC_{50} 3.08 μM) showed two times more

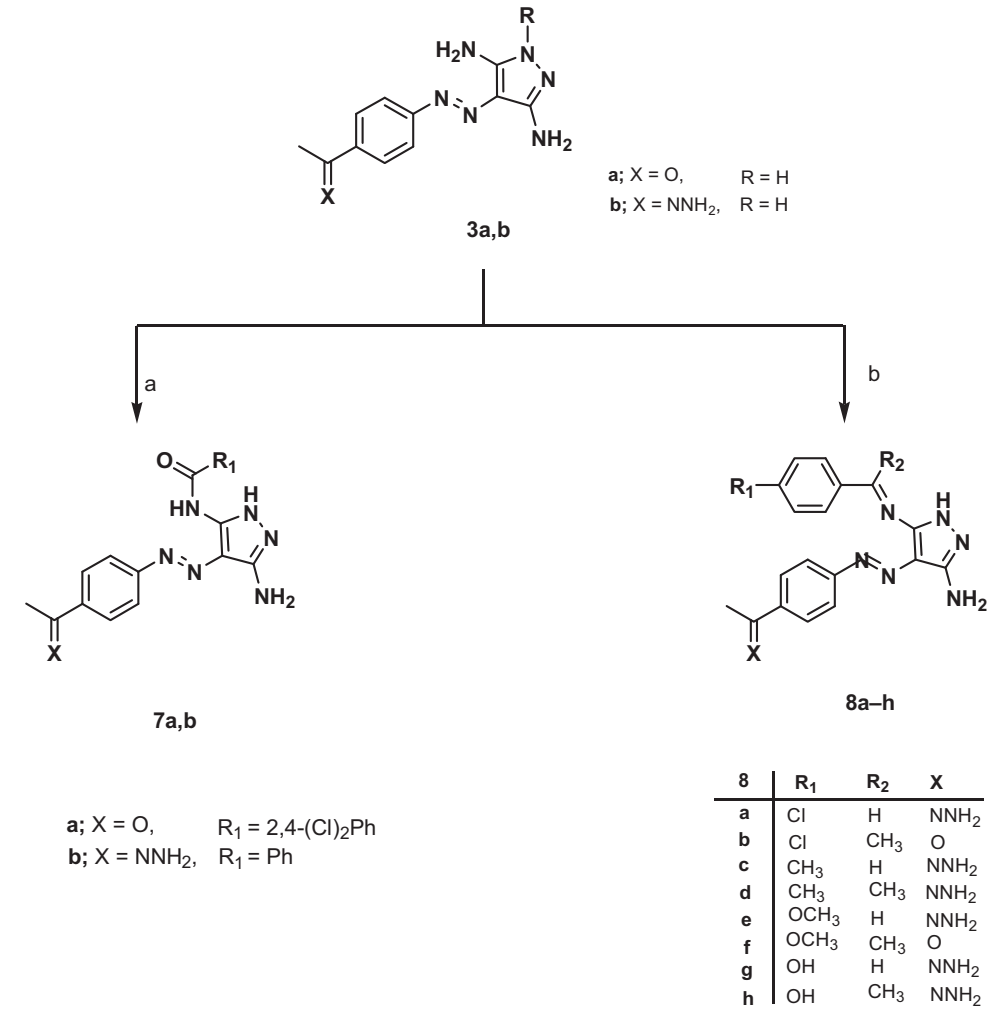

8	R_1	R_2	X
a	Cl	H	NNH_2
b	Cl	CH_3	O
c	CH_3	H	NNH_2
d	CH_3	CH_3	NNH_2
e	OCH_3	H	NNH_2
f	OCH_3	CH_3	O
g	OH	H	NNH_2
h	OH	CH_3	NNH_2

SCHEME 2 The synthesis of compounds **7a,b** and **8a–h**. Reagents and conditions: (a) RCOCl, DMF, stirring; (b) aromatic aldehydes or ketones, EtOH, fused Na acetate, reflux, 3 hr

potent cytotoxicity than imatinib (IC_{50} 6.00 μM). Another promising analog, **8f** (IC_{50} 4.03 μM), elicited 1.5-fold activity than imatinib. It is interesting to note that **8b** and **8f** bearing 4-acetyl on aryl moiety were the most potent hits among our study. Both have $R_2 = CH_3$, so condensation with acetophenones is preferable than aldehydes among all prepared Schiff bases. It is worth mentioning that in the case of **8b**, R_1 = Cl, whereas in the case of **8f**, $R_1 = OCH_3$, which means that the electronic effect is not essential for activity. Among all inactive analogs having hydrazono-ethyl instead of 4-acetyl on the aryl moiety, **8d** (R_1, $R_2 = CH_3$) showed a moderate activity (IC_{50} 38.9 μM) and **8g** (R_1 = OH, R_2 = H) elicited mild cytotoxicity (IC_{50} 69.1 μM).

2.2.2 | Effect on cell cycle arrest on MCF-7 cells

The most active compound **8b** was selected for more study for its effect on cell cycle progression in the MCF-7 cell line. The MCF-7 cells were incubated for 24 hr with **8b** concentrations of IC_{50}, and their effect on the normal profile of the cell cycle was analyzed. Exposure of MCF-7 cells to **8b** resulted in an interference with the normal cell cycle distribution of this cell line. The cells in the S phase, control group, accounted for about 23.59%, whereas after cells were treated with compound **8b**, the ratio was approximately 33.08%. This shows that the cells were arrested in the S phase, as shown in Table 2. Such an increase came with a reduction of cells at both the G0/G1 and G2/M phases of the cell cycle. Moreover, treatment with **8b** produced a significant increase in pre-G1 phase percent by four-fold, which resulted in interference with the normal cell cycle and was indicative of apoptosis. The results were represented by a bar chart that shows the percentage of MCF-7 cells at each stage of the cell cycle in control cells and **8b**-treated cells (Figure 3a,b and Table 2).

2.2.3 | Annexin V-fluorescein isothiocyanate (FITC) apoptosis assay

Apoptosis induction by **8b** following S-phase arrest was assessed by the Annexin V-FITC apoptosis assay. One of the earliest cellular changes evident during apoptosis is the translocation of

TABLE 1 IC_{50} values of compounds **3–8** against MCF-7 cells

Cpd no.	R_1	R_2	X	IC_{50} (μM)
3a	H	–	O	26.86 ± 0.54
3b	H	–	NNH_2	>100
3c	Ph	–	O	>100
4a	Antipyrin-4-yl	–	O	34.7 ± 14.78
4b	2-Naphthol-1-yl	–	NNH_2	>100
6a	H	–	O	>100
6b	Ph	–	O	38.7 ± 3.50
7a	2,4-$(Cl)_2$Ph	–	O	13.8 ± 0.56
7b	Ph	–	NNH_2	>100
8a	Cl	H	NNH_2	>100
8b	Cl	CH_3	O	3.08 ± 0.15
8c	CH_3	H	NNH_2	>100
8d	CH_3	CH_3	NNH_2	38.9 ± 1.53
8e	OCH_3	H	NNH_2	>100
8f	OCH_3	CH_3	O	4.03 ± 0.28
8g	OH	H	NNH_2	69.1 ± 10
8h	OH	CH_3	NNH_2	>100
Imatinib				6.00 ± 0.53
CAN508				62.00 ± 8.00

phosphatidylserine (PS) from the inner to the outer side of the plasma membrane.[21] Fluorescently labeled annexin V, which binds to phosphatidylserine,[22] can be used as a sensitive probe for PS in the outer leaflet of the plasma membrane.[23] Also, propidium iodide (PI), a fluorescent molecule binding to nucleic acids, but which does not enter live cells, can be used to counterstain dead cells. To differentiate between apoptosis and necrosis, both annexin V-FITC and PI staining are usually performed. Annexin V/PI staining was performed in cells exposed to **8b** for 24 hr. The results revealed that the application of compound **8b** on MCF-7 cells for 24 hr increases the early apoptosis ratio (lower right quadrant of the cytogram) from 0.42% to 7.64% and increases the late apoptosis ratio (higher right quadrant of the cytogram) from 0.39% to 18.73%. This means that compound **8b** induced apoptosis almost up to 32.5-fold, both early and late cellular apoptosis when compared with the control. These data suggest that compounds **8b** triggered apoptosis via the programmed cell death pathway rather than a necrotic pathway (Table 3 and Figure 4).

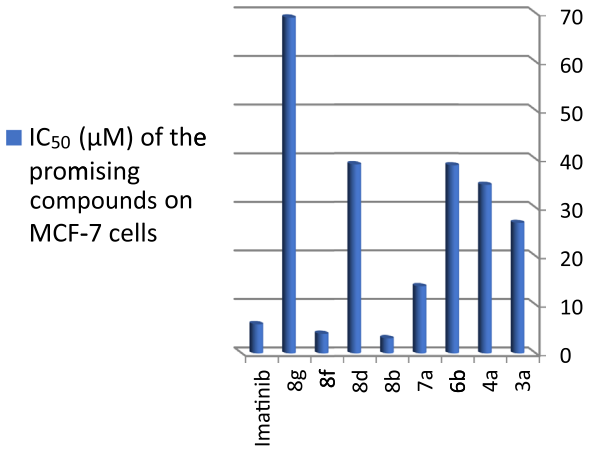

FIGURE 2 IC_{50} values of the promising derivatives against the MCF-7 cell line

TABLE 2 Cell cycle distribution after treatment with compound **8b**

	Cell cycle distribution (%)			
Cpd no.	Pre-G	G0/G1	S	G2/M
Control	3.09	69.37	23.59	7.04
8b	12.64	63.54	33.08	3.38

2.2.4 | CDK2/cyclin E kinase inhibitory activity

To explore the mechanism of action of **8b**, CDK2/cyclin E in vitro assay was performed using imatinib and CAN508. The obtained results revealed that **8b** showed a good inhibitory effect (IC_{50} 0.24 μM) on CDK2/cyclin E enzyme, compared with imatinib (IC_{50} 0.15 μM), which are both more potent than CAN508 (Table 4).

2.3 | Molecular modeling studies

2.3.1 | Docking with CDK2

Table 3 displays docking scores and bond interactions of ligand **X**, the 3,5-diaminopyrazole CDK2-inhibitor, and the target compound **8b** with amino acids of CDK2 active site. Furthermore, Figure 5a,b represent interactions with the amino acids of CDK2 in 2D and 3D styles, respectively.

In this study, the docked model of lead compound **X** with CDK2 showed that compound **X** bonded to the active site via three hydrogen bond donors with Ile10, Leu83, and Gln131. The pyrazole moiety faces Lys 89 by arene–cation interaction. Moreover, hydrophobic interaction with Ile10 and Leu134 was observed.

Docking study of compound **8b** showed higher affinity in the active site of CDK2 (ΔG = −5.6 kcal/mol) than that of the ligand (ΔG = −4.4 kcal/mol).

The binding mode of **8b** was revealed in Figure 6a,b, where pyrazole scaffold binds to the active site of CDK2 via three hydrogen bonds. Two hydrogen bond donors are between ^{1}N, ^{2}N of pyrazole and the CDK amino acids Leu83 and Glu81, respectively. Another hydrogen bond acceptor is between ^{2}N of pyrazole and amino acid Leu83. Compound **8b** has the same binding mode as previously reported inhibitors with the same pyrazole core.

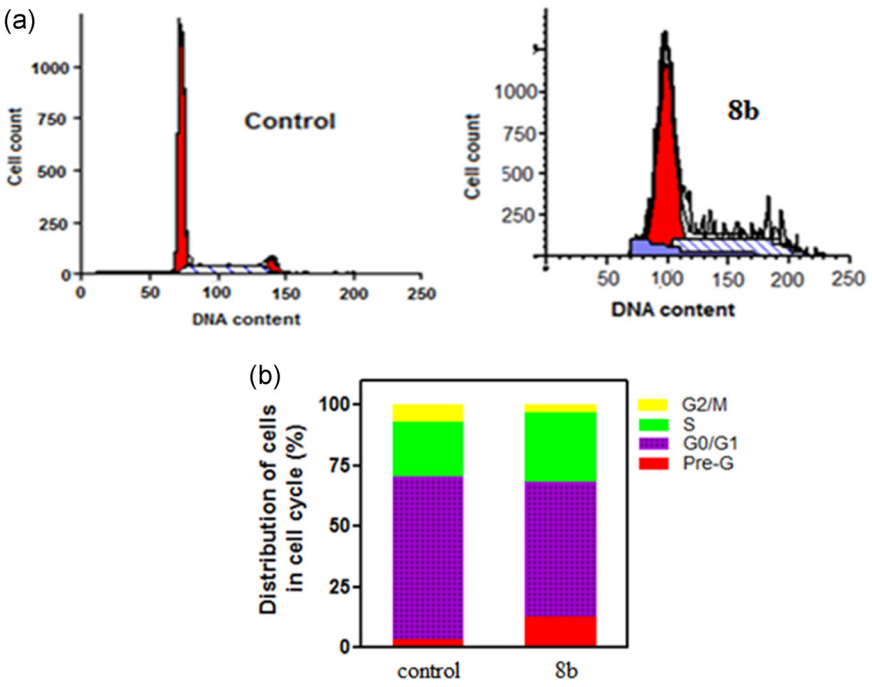

FIGURE 3 (a) The effect of **8b** on DNA ploidy of MCF-7 cells by flow cytometric analysis. (b) Bar chart showing the percentage of MCF-7 cells in control cells and **8b**-treated cells at each stage of the cell cycle

The aryl moiety attached at position 5 of the pyrazole ring creates hydrophobic interactions with the side chain of Ile10, Lys 89, and Gln131 residues. More hydrophobic interactions occurred between the acetophenone moiety and the amino acids Asp145 and Leu134.

2.3.2 | 3D-QSAR pharmacophore modeling

The 3D-QSAR Pharmacophore Generation protocol (HypoGen protocol of CATALYST; 13) was applied using Discovery Studio 2.5 software to create 10 predictive pharmacophore models via aligning different conformations in which the molecules were likely to bind with the receptor pharmacophore models.[24]

The given hypothesis was combined with known activity data to create a 3D-QSAR model that identifies overall aspects of molecular structure governing the activity. During hypothesis generation, the structure and activity correlations in the training set were rigorously examined. HypoGen identifies features common to the active compounds and excludes features common to the inactive compounds within a conformationally allowable region of space. It further estimates the activity of the newly synthesized and tested compounds using regression parameters. The parameters were calculated by regression analysis, using the correlation of the geometric fit value contrasted with the biological activity. The better the geometric fit, the greater is the activity prediction of the compound. The fit function checks if the feature is mapped. It also contains a distance term, which measures the distance breaking the feature on the molecule from the centroid of the feature in the pharmacophore hypothesis. Both terms are used to calculate the geometric fit value.[25]

TABLE 3 The effect of **8b** on annexin V-fluorescein isothiocyanate-positive staining in MCF-7 cells

	Apoptosis in MCF-7 cells			
Cpd no.	Total	Early	Late	Necrosis
8b	28.36	7.64	18.73	1.99
Control	1.79	0.42	0.39	0.98

Pharmacophore study results

In this study, pharmacophore models were generated using two hydrogen bond acceptors (HBA), hydrophobic (Hyd), and ring aromatic (RA) features, and nine pharmacophore models were exported for further studies. All the generated pharmacophore models contained at least two chemical features. The best-generated pharmacophore contained two HBA features, 1 ring aromatic, and 1 hydrophobic feature (Figure 7). The constraint distances and angles between the different features of the generated top pharmacophore are presented in Table 5.

The diazo linker and C═O group contribute to the pharmacophore by two HBA features, and the methyl group of the 5-ethylidene amino moiety represents a hydrophobic feature, in addition to the phenyl group of the acetophenone moiety, which acts as an aromatic ring feature, as shown in Figure 8.

The best-generated pharmacophore significance was 98%. The top pharmacophore hypothesis generated was developed with a total cost value of 104.77, null cost = 226.1, and fixed cost = 59.75. Further evaluation of the generated pharmacophore models was based on the correlation coefficient,[26] which was found to be 0.869, indicating the capability of the pharmacophore model to predict the activity of the training set compounds. The predicted activities through the pharmacophore model are represented in Table 6 as well as their fit

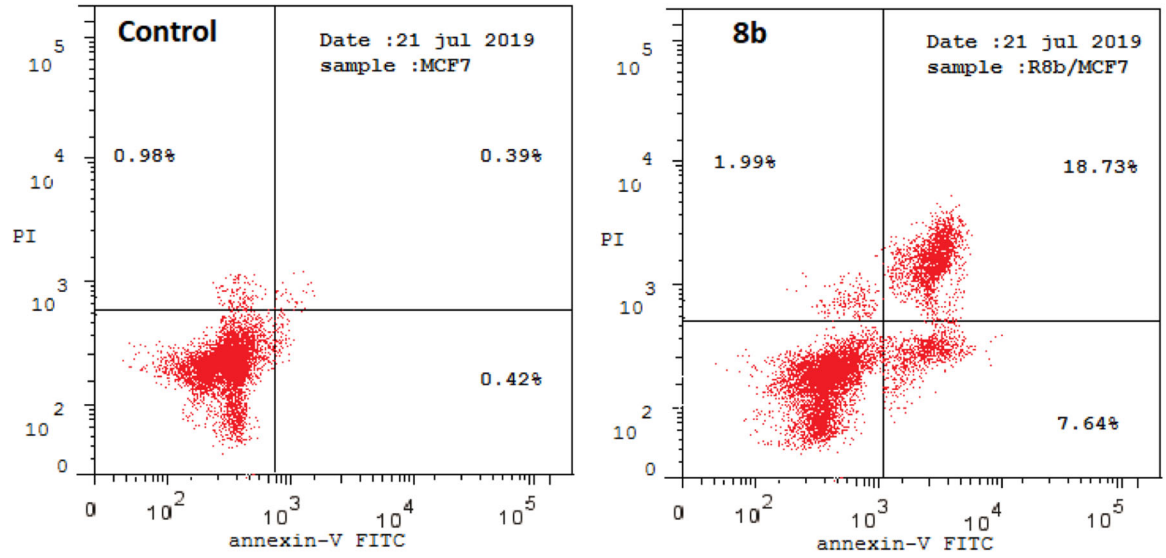

FIGURE 4 The effect of **8b** on MCF-7 cell death

TABLE 4 CDK2 inhibitory activity of compound **8b**

Cpd no.	IC_{50} (μM)
Imatinib	0.15 ± 5.92
CAN508	20 ± 6.00
8b	0.24 ± 9.55

values. Furthermore, compound **8b** was mapped into the best-generated pharmacophore model, using a ligand pharmacophore mapping protocol, with fit value = 6.85.

Validation of 3D-QSAR pharmacophore

Validation of the obtained pharmacophore model was carried out using cost analysis and Fischer validation test for activity prediction. HypoGen selects the best hypotheses by applying a cost analysis. The overall cost of each hypothesis is calculated by summing three cost factors—a weight cost, an error cost, and a configuration cost. HypoGen also calculates two theoretical costs, the null and fixed costs, which can be used to determine the significance of the selected hypotheses. The cost values of the optimized hypotheses should lie between these two costs. A larger difference between the fixed and null costs than that between the fixed and total costs signifies the quality of a pharmacophore model. The closer the cost value to the fixed cost and the further away it is from the null cost, the more significant the hypothesis might be.

Fischer validation is another method for pharmacophore model validation. This validation method checks the correlation between chemical structures and biological activity. It also generates pharmacophore hypotheses using the same parameters as those used to

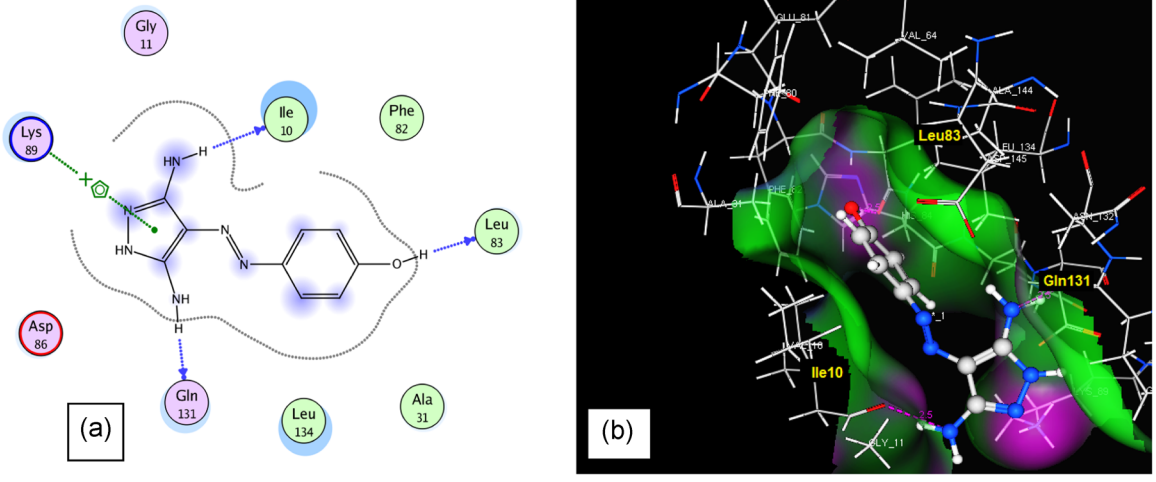

FIGURE 5 The proposed ligand **X** binding mode docked in the active CDK2 site. (a) Two-dimensional ligand–receptor interactions and (b) three-dimensional ligand–receptor interactions (C atoms are gray, N atoms are blue, and O atoms are red). The important amino acid residues are shown together with their respective numbers. Compound **X** formed three hydrogen bonds with Ile10, Leu83, and Gln131

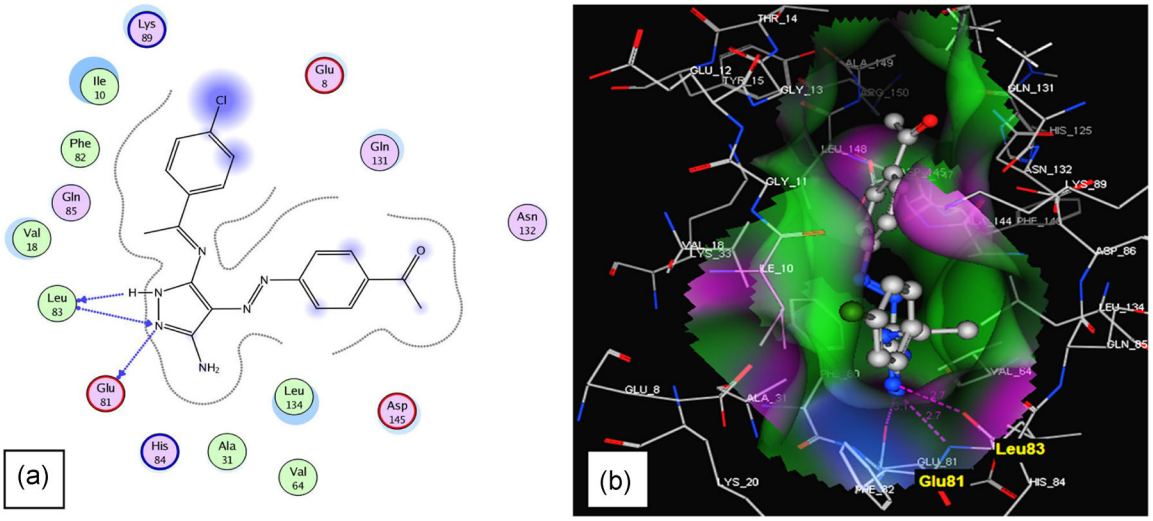

FIGURE 6 The proposed **8b** binding mode docked in the active CDK2 site. (a) Two-dimensional ligand–receptor interactions and (b) three-dimensional ligand–receptor interactions (C atoms are gray, N atoms are blue, and O atoms are red). The important amino acid residues are shown together with their respective numbers. Compound **8b** formed three hydrogen bonds with Leu83 and Glu81

develop the original pharmacophore hypothesis by randomizing the activity data of the training set compounds. The Fischer validation confidence level chosen was 98%. In addition to cost analysis and Fischer validation, the pharmacophore model was validated through activity prediction of the synthesized structures as the training set.

2.3.3 | In silico evaluation of physicochemical and absorption, distribution, metabolism, and excretion (ADME) properties

A computational study of the synthesized compounds was performed to evaluate physicochemical properties, ADME, and ligand efficiency data using SwissADME,[27] Molsoft,[28] and Pre-ADME[29] websites, and DataWarrior software.[30] With respect to physicochemical properties (Table 7), all the synthesized compounds have zero violations for Lipinski's rule for oral drugs. Also, according to the screening process with Veber rules, all the hits meet the criteria of drug-likeness, except compound **4a**, which did not obey Veber rules regarding TPSA (<140). Additionally, absorption (%ABS) was estimated by using the following equation: %ABS = 109 − (0.345 × TPSA),[33] and it was found that the calculated % ABS of all these hits ranged between 52.87885% and 88.43455%, demonstrating that these synthesized derivatives may have the required cell membrane permeability and bioavailability. All compounds have rotatable bonds between 3 and 6, which indicates molecular flexibility to their biotarget. Curiously, all the screened derivatives are not substrates of P-gp protein, so they have a minor chance of efflux out of the cell, thus resulting in a maximum effect. Furthermore, all the screened analogs have no permeation to the blood–brain barrier, except compound **6b**, thus ensuring that these systemically targeted molecules will have low to no side effects on the central nervous system.

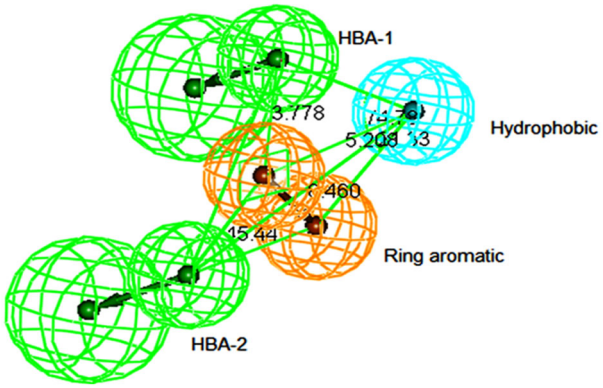

FIGURE 7 Constraint distances and angles between features of the generated top pharmacophore model with the features considered hydrogen bond acceptors (HBA1 and HBA2) colored in green, aromatic ring (RA) colored in orange, and hydrophobic colored in cyan

TABLE 5 Constraint distances and angles between features of the generated top pharmacophore model

Constraint distances (Å)	Constraint angles (°)
HBA1–HBA2: 7.18	HBA1, HBA2, RA: 45.59
RA–HBA1: 3.77	HBA1, Hyd, RA: 74.78
RA–HBA2: 3.69	HBA2, Hyd, RA: 21.38
Hyd–RA: 5.20	
Hyd–HBA1: 4.13	
Hyd–HBA2: 8.46	

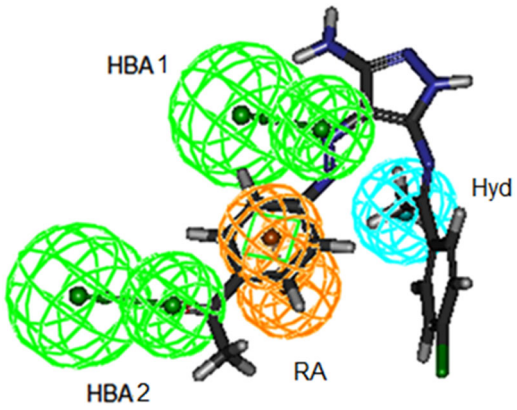

FIGURE 8 The best-generated pharmacophore hypothesis with the features considered hydrogen bond acceptors (HBA1 and HBA2) colored in green, ring aromatic (RA) colored in orange, hydrophobic (Hyd) colored in cyan, and the synthesized structure **8b** fitted in the pharmacophore with fit value 6.85

Bioavailability is an index of the amount of drug present in the plasma and is considered as the most crucial factor affecting absorption.[34] Interestingly, it has been found that all the screened derivatives have high bioavailability scores. Synthetic accessibility scores of all the analogs were found to be between 2.47 and 4.24, indicating that they can be readily synthesized on a large scale.

In pan assay interference compounds (PAINS) structural alert, all the compounds were found to have only one structural alert (azo group). Although PAINS are important features to be considered while developing drugs to avoid false-positive results, yet overestimation and blind use of these filters might only lead to the exclusion of promising hits based on phantom PAINS.[35]

Additionally, Molsoft software was used to estimate the solubility score of the screened derivatives, and it was found that these derivatives fulfilled the requirements of the solubility with values in the range of 14.04–2,993.99 mg/l (more than 0.0001 mg/l)

The Pre-ADME server has been used to assess the intestinal absorption, identify potential drugs for oral delivery, and give information regarding the therapeutic drugs in the central nervous system and plasma–protein binding (PPB) model in its disposition and efficacy.[36]

The in silico assessment results of pharmacokinetic parameters, Caco2 permeability coefficient, HIA, and PPB of the selected molecules, were obtained from the Pre-ADMET server. As shown in Table 7, all the screened compounds showed medium cell permeability in the Caco-2 cell model, with values between 6.13254 and 31.9615 nm/s, except **3a** and **8f**, which display low cell permeability, 0.43128 and 1.27469 nm/s, respectively. Also, they revealed high human intestinal absorption values (78.427541–97.802862%), indicating very well-absorbed compounds. According to the analysis of the PPB abilities, all compounds showed high protein binding (90.456917–99.845118%), except **3a** and **8f**, which displayed low protein binding, 69.716397 and 82.451914, respectively.

It has been established that increased molecular weight and lipophilicity result in improved binding potency, but in the meantime, they are closely correlated to increased binding promiscuity and diminished safety thresholds. Ligand efficiency (LE) and lipophilic ligand efficiency (LLE) are two parameters describing the balance between potency and molecular size, which is related to various pharmacokinetic and toxicological parameters.[37,38] LE (= 1.37 [pIC_{50}]/non-hydrogen atoms)[39] measures the average binding energy per non-hydrogen atom instead of considering the binding affinity of the whole molecule. Thus, it allows comparing and prioritizing ligands corrected for their sizes, and LLE (= pIC_{50} − cLogP) is a measure of how efficiently a ligand can exploit its lipophilicity to bind to its target.[40] So LLE monitoring highlights the price paid in ligand lipophilicity at the expense of its potency. Herein, LE and LLE values of the most active compound **8b** were calculated on the basis of its IC_{50} values against the screened enzyme assays (CDK2/cyclin E). The results (Table 7) indicated that **8b** had an acceptable limit, 0.33572, >0.3. Additionally, **8b** showed an accepted LLE value, 3.0375. Collectively, and based on the estimated physicochemical properties, ADME, and LE predictors, these active compounds considered as a pharmacologically active framework should be considered for developing further potential hits.

TABLE 6 Fit values and estimated activities for the synthesized compounds mapped with the generated three-dimensional pharmacophore model

Cpd. no.	Predicted activity, IC_{50} (μM)	Experimental activity, IC_{50} (μM)	Fit values
3a	140.01	26.6	5.21
3b	1.42	1,120.6	4.20
3c	139.46	485.6	5.22
4a	58.98	239.9	5.59
4b	386.25	246.6	4.77
6a	137.95	107	5.22
6b	138.18	38.5	5.22
7a	41.44	13.6	5.74
7b	771.88	680.3	4.47
8a	460.31	380	4.70
8b	3.20	3.1	6.85
8c	468.06	425.3	4.69
8d	51.01	39.3	5.65
8e	248.36	1,248.3	4.96
8f	3.00	4.1	6.88
8g	47.47	69	5.68
8h	50.62	154.9	5.66

3 | CONCLUSION

In the process of anticancer drug discovery, to find new potential antibreast cancer agents, we synthesized a novel series of pyrazole derivatives. The antiproliferative activity of new derivatives was

TABLE 7 In silico physicochemical properties, ADME (absorption, distribution, metabolism, and excretion), and ligand efficiency data of the active compounds

	Compd. no.					
	3a	**4a**	**6b**	**7a**	**8b**	**8f**
SWISS ADME						
MW	244.25	415.41	318.37	417.25	380.83	376.41
MlogP	0.42	1.59	2.76	2.4	3.06	2.27
HBD	3	3	0	3	2	2
HBA	4	8	4	5	5	6
Lipinski's violation	0	0	0	0	0	0
No. of rotatable bonds	3	6	4	6	5	6
TPSA	122.51	162.67	59.61	125.59	108.85	118.08
%ABS	66.73405	52.87885	88.43455	65.67145	71.44675	68.2624
Veber rule	0	1	0	0	0	0
P-gp substrate	No	No	No	No	No	No
BBB	No	No	Yes	No	No	No
Bioavailability score	0.55	0.55	0.55	0.55	0.55	0.55
Synthetic accessibility	2.47	4.24	2.9	2.99	3.35	3.44
PAINS	1	1	1	1	1	1
Molsoft						
S (mg/l)	2,993.99	92.57	15.33	52.42	14.04	36.36
Pre-ADME						
Caco2[a]	0.43128	6.13254	31.9615	13.9876	14.7366	1.27469
HIA[b]	83.800246	78.427541	97.802862	89.232413	91.575738	90.257977
PPB[c]	69.716397	92.399604	90.456917	99.845118	95.372135	82.451914
DataWarrior						
LE[d](CDK2/cyclin E)	–	–	–	–	0.33572	–
LLE[e]	–	–	–	–	3.0375	–

Abbreviations: %ABS, percentage of absorption; BBB, blood–brain barrier; Caco2, permeability through cells derived from human colon adenocarcinoma; HBA, the number of hydrogen bond acceptors; HBD, the number of hydrogen bond donors; HIA, percentage human intestinal absorption; LE, ligand efficiency; LLE, lipophilic ligand efficiency; LogP, logarithm of compound partition coefficient between *n*-octanol and water; MW, molecular weight; PPB, plasma–protein binding; *S*, aqueous solubility; TPSA, topological polar surface area.

[a]Caco2 values < 4 nm/s (low permeability), values ranged from 4 to 70 nm/s (medium permeability), and values >70 nm/s (high permeability).

[b]HIA values ranged from 0% to 20% (poorly absorbed), values ranged from 20% to 70% (moderately absorbed), and ranged from 70% to 100% (well-absorbed).

[c]PPB values <90% (poorly bound) and values >90% (strongly bound).

[d]The lowest acceptable limit is 0.3.[31]

[e]Values ≥3 are acceptable for lead compounds, whereas drug-like candidates record values ≥5.[32]

examined against MCF-7 breast cancer using the 3-(4,5-dimethylthiazole-2-yl)-2,5-diphenyltetrazolium bromide (MTT) technique. Compound **8b** was the most active member against MCF-7 cells, showing an IC_{50} value of 3.08 μM. Biological assessment using flow cytometric analysis revealed that it induced apoptosis and cell cycle arrest at S phase and exhibited 62.5% inhibition of CDK2/cyclin E as compared with imatinib. Moreover, 3D-QSAR pharmacophore modeling showed the importance of the diazo linker and C═O of acetophenone moiety as 2HBA features; ring aromatic was also important. Additionally, the methyl group of ethylidene amino moiety was an essential hydrophobic feature. Finally, a combination of 3D pharmacophore modeling and cytotoxicity results would provide an effective technique for understanding the observed pharmacological properties, which might, thus, be adopted for developing effective lead structures.

4 | EXPERIMENTAL

4.1 | Chemistry

4.1.1 | General

All chemicals were bought from VWR International Merck, Germany, or Sigma-Aldrich and utilized without further purification. Melting points were determined with an open capillary tube method using Stuart SMP3 Melting Point apparatus, and they were uncorrected. Elemental microanalysis was carried out at the Regional Center for Mycology and Biotechnology, Al-Azhar University. Infrared spectra were recorded on a Shimadzu infrared spectrometer IR Affinity-1 (FTIR-8400S-Kyoto-Japan) and expressed as wavenumber (cm^{-1}),

using potassium bromide discs at the Armed Forces Laboratories. ^{1}H NMR (nuclear magnetic resonance) spectra were recorded on a Varian Gemini 300-MHz spectrophotometer; the spectra were run at 300 MHz in deuterated dimethylsulfoxide (DMSO-d_6) at the Armed Forces Laboratories. ^{13}C NMR spectra were recorded on a Varian Gemini 300 MHz spectrophotometer, and the spectra were run at 300 and 400 MHz in DMSO-d_6 at the Armed Forces Laboratories. Chemical shifts were expressed in δ units and were related to that of the solvents. As for the proton magnetic resonance, D_2O was carried out for NH and OH exchangeable protons. Mass spectra (MS) were recorded using a Shimadzu gas chromatograph mass spectrometer-Qp 2010 plus (Japan) and were carried out at the Regional Center for Mycology and Biotechnology, Al-Azhar University. All the reactions were followed by thin-layer chromatography using silica gel F254 plates (Merck) and were visualized by an ultraviolet (UV) lamp. The intermediates **2** and **5** are prepared according to the reported method,[41,42] as well as compounds **3a,b**.[12]

The InChI codes of the investigated compounds, together with some biological activity data, are provided as Supporting Information.

4.1.2 | Synthesis of 1-{4-[(3,5-diamino-1-phenyl-1*H*-pyrazol-4-yl)diazenyl]phenyl}ethanone (3c)

A mixture of equimolar amounts of 2-[(4-acetylphenyl)diazenyl] malononitrile **2** and phenylhydrazine was refluxed in ethanol (95%, 30 ml) for 4 hr and then poured after cooling into ice-cold water to produce **3c**. The solid product so formed was filtered off and crystallized from ethanol. M.p. 218–220°C; yield 64%; IR (KBr, cm^{-1}): 3,466, 3,414, 3,346, 3,280 (2NH_2), 1,672 (C═O), 1,625 (C═N), and 1,596 (N═N); ^{1}H NMR (300 MHz, DMSO-d_6) δ (ppm): 2.58 (s, 3H, CH_3), 5.95 (s, 2H, NH_2, D_2O-exchangeable), 6.76–7.49 (m, 3H, Ph-H), 7.56 (d, 2H, Ph-$H_{2,6}$, J = 8.4 Hz), 7.74 (d, 2H, Ph-$H_{3,5}$, J = 8.4 Hz), 7.82 (d, 2H, Ph-H), and 9.30 (s, 1H, NH, D_2O-exchangeable); ^{13}C NMR (100 MHz, DMSO-d_6) δ (ppm): 21.81, 72.40, 112.64, 112.96, 118.70, 120.52, 122.08, 125.63, 129.31, 137.81, 138.44, 140.24, 146.00, 152.55, and 196.96; MS [*m*/*z*, %]: 320 [M$^+$, 16.03]; Anal. calcd. for $C_{17}H_{16}N_6O$ (%): C, 63.74; H, 5.03; N, 26.23. Found: C, 63.88; H, 5.11; N, 26.49.

4.1.3 | General procedure for the synthesis of compounds 4a,b

A solution of β-naphthol or 3-phenyl-1*H*-pyrazol-5(4*H*)-one (0.1 mol) in ethanol (100 ml) was treated with a suspension of sodium acetate (0.1 mol in 50 ml of H_2O). A solution of diazonium salt of **3a** or **3b** (0.1 mol) in acetic acid (50 ml) was then added, with stirring the previous mixture. The solid products, obtained on standing, were collected by filtration and washed several times with hot water and recrystallized from ethanol.

*4-({4-[(4-Acetylphenyl)diazenyl]-3-amino-1H-pyrazol-5-yl}diazenyl)-3-phenyl-1H-pyrazol-5(4H)-one (**4a**)*

M.p. >300°C; yield 50%; IR (KBr, cm^{-1}): 3,400–3,200 (br. NH_2, NH), 1,690 (CO), 1,666 (CON), and 1,594 (N═N); ^{1}H NMR (300 MHz, DMSO-d_6) δ (ppm): 2.64 (s, 3H, CH_3), 7.05 (s, 2H, NH_2, D_2O-exchangeable), 7.40–8.17 (m, 9H, 4Ar-H, 5Ph-H), 12.27 (s, 1H, NH, D_2O-exchangeable), 12.39 (s, 1H, NH, D_2O-exchangeable), and 12.89 (s, 1H, NH, D_2O-exchangeable); ^{13}C NMR (100 MHz, DMSO-d_6) δ (ppm): 26.70, 99.40, 118.89, 121.81, 126.58, 126.82, 128.58, 129.51, 130.05, 144.58, 160.00, and 196.55; MS [*m*/*z*, %]: 415 [M$^+$, 0.22]; Anal. calcd. for $C_{20}H_{17}N_9O_2$ (%): C, 57.83; H, 4.12; N, 30.35. Found: C, 57.96; H, 4.17; N, 30.49.

*1-[4-({3-Amino-5-[(2-hydroxynaphthalen-1-yl)diazenyl]-1H-pyrazol-4-yl}diazenyl) phenyl]ethanone (**4b**)*

M.p. 147–150°C; yield 55%; IR (KBr, cm^{-1}): 3,385–2,740 (OH, NH, NH_2), 1,625 (C═N), 1,598 (N═N); ^{1}H NMR (300 MHz, DMSO-d_6) δ (ppm): 2.57 (s, 1H, OH, D_2O-exchangeable), 2.61 (s, 3H, CH_3), 6.73–8.50 (m, 12H, 10Ar-H, NH_2), and 15.87 (s, 1H, NH, D_2O-exchangeable); MS [*m*/*z*, %]: 413 [M$^+$, 5.00]; Anal. calcd. for $C_{21}H_{19}N_9O$ (%): C, 61.01; H, 4.63; N, 30.49. Found: C, 61.17; H, 4.70; N, 30.72.

4.1.4 | General procedure for the synthesis of compounds 6a,b

A mixture of **5** (0.01 mol) and hydrazine hydrate 98% or phenylhydrazine (0.015 mol) in glacial acetic acid (15 ml) was refluxed for 4–5 hr. The resulting mixture was concentrated and allowed to cool. Then the resulting solid so formed was filtered, washed, dried, and crystallized from ethanol.

1-{4-[(3,5-Dimethyl-1H-pyrazol-4-yl)diazenyl]phenyl}ethanone (6a)

M.p. 109–110°C; yield 65%; IR (KBr, cm^{-1}): 3,322 (NH), 1,651 (C═O), and 1,555 (N═N); ^{1}H NMR (300 MHz, DMSO-d_6) δ (ppm): 1.82 (s, 6H, 2CH_3), 2.58 (s, 3H, $COCH_3$), 7.79 (d, 2H, Ph-$H_{3,5}$, J = 8.4 Hz), 8.07 (d, 2H, Ph-$H_{2,6}$, J = 8.4 Hz), and 9.64 (s, 1H, NH, D_2O-exchangeable); ^{13}C NMR (100 MHz, DMSO-d_6) δ (ppm): 19.58, 20.88, 27.27, 121.79, 129.90, 135.15, 137.18, 156.07, 168.40, and 197.72; MS [*m*/*z*, %]: 242 [M$^+$, 100]; Anal. calcd. for $C_{13}H_{14}N_4O$ (%): C, 64.45; H, 5.82; N, 23.13. Found: C, 64.62; H, 5.89; N, 23.21.

*1-{4-[(3,5-Dimethyl-1-phenyl-1H-pyrazol-4-yl)diazenyl]phenyl}-ethanone (**6b**)*

M.p. 82–85°C; yield 64%; IR (KBr, cm^{-1}): 1,653 (C═O), 1,592 (C═N), and 1,558 (N═N); ^{1}H NMR (300 MHz, DMSO-d_6) δ (ppm): 2.27 (s, 3H, CH_3), 2.44 (s, 3H, CH_3), 2.65 (s, 3H, $COCH_3$), 7.68–7.74 (m, 5H, Ph-H), 7.79 (d, 2H, Ph-$H_{3,5}$, J = 8.4 Hz), and 8.07 (d, 2H, Ph-$H_{2,6}$, J = 8.4 Hz); ^{13}C NMR (100 MHz, DMSO-d_6) δ (ppm): 20.34, 20.40, 26.85, 121.31, 121.43, 129.40, 134.66, 136.70, 155.58, 167.89, 173.95, and 197.22; MS [*m*/*z*, %]: 318 [M$^+$, 0.50]; Anal. calcd. for $C_{19}H_{18}N_4O$ (%): C, 71.68; H, 5.70; N, 17.60. Found: C, 71.85; H, 5.76; N, 17.83.

4.1.5 | General procedure for the synthesis of compounds 7a,b

Equimolar amounts of **3a** or **3b** reacted with benzoyl chloride or 2,4-dichlorobenzoyl chloride by stirring in DMF (15 ml) at room temperature for 2 hr, and then the mixture was poured into water (30 ml) and neutralized with few drops of HCl. The resulted solid was then filtered and dried.

*N-{4-[(4-Acetylphenyl)diazenyl]-3-amino-1H-pyrazol-5-yl}-2,4-dichlorobenzamide (**7a**)*

M.p. 118–120°C; yield 44%; IR (KBr, cm^{-1}): 3,421, 3,344 (NH_2), 3,172 (NH), 1,718 (Ar–C═O), 1,641 (CH_3–CO), 1,612 (C═N), and 1587 (N═N); ^{1}H NMR (300 MHz, DMSO-d_6) δ (ppm): 2.56 (s, 3H, CH_3), 6.37 (s, 2H, NH_2, D_2O-exchangeable), 7.58–7.76 (m, 4H, Ar-H), 7.84–8.00 (m, 3H, Ar-H), and 8.40 (s, 1H, NH, D_2O-exchangeable); ^{13}C NMR (100 MHz, DMSO-d_6) δ (ppm): 27.22, 76.18, 121.61, 127.60, 129.73, 129.91, 130.33, 130.88, 134.50, 136.40, 147.13, 149.44, 152.40, 156.14, 157.36, 161.16, 161.55, and 197.36; MS [*m*/*z*, %]: 417 [M^++1, 0.23]; Anal. calcd. for $C_{18}H_{14}Cl_2N_6O_2$ (%): C, 51.81; H, 3.38; N, 20.14. Found: C, 51.99; H, 3.46; N, 20.42.

*N-(3-Amino-4-{[4-(1-hydrazonoethyl)phenyl]diazenyl}-1H-pyrazol-5-yl)benzamide (**7b**)*

M.p. 107–110°C; yield 42%; IR (KBr, cm^{-1}): 3,330, 3,260 (br., $2NH_2$, 2NH), 1,676 (C═O), 1,604 (C═N), and 1,576 (N═N); ^{1}H NMR (300 MHz, DMSO-d_6) δ (ppm): 2.42 (s, 3H, CH_3), 7.42–7.64 (m, 7H, Ar-H), 7.91 (d, 2H, Ph-$H_{2,6}$), and 12.86 (s, 1H, NH, D_2O-exchangeable); ^{13}C NMR (100 MHz, DMSO-d_6) δ (ppm): 26.32, 125.07, 126.84, 128.40, 128.59, 129.14, 129.23, 130.69, 132.75, 132.87, and 167.23; MS [*m*/*z*, %]: 362 [M^+, 9.77]; Anal. calcd. for $C_{18}H_{18}N_8O$ (%): C, 59.66; H, 5.01; N, 30.92. Found: C, 59.80; H, 5.12; N, 31.14.

4.1.6 | General procedure for the synthesis of compounds 8a–h

An equimolar amount of **3a** or **3b** (0.01 mol) was refluxed with different aromatic aldehydes or aromatic acetophenones in ethanol (20 ml)/fused sodium acetate (0.2 g) for 3–5 hr, and then the formed solid product was collected by filtration and washed with hot ethanol.

*4-Chlorobenzylidene-4-{[4-(1-hydrazonoethyl)phenyl]diazenyl}-1H-pyrazole-3,5-diamine (**8a**)*

M.p. 210–213°C; yield 50%; IR (KBr, cm^{-1}): 3,453, 3,388, 3,277 (NH, NH_2), 1,613 (C═N), and 1562 (N═N); ^{1}H NMR (300 MHz, DMSO-d_6) δ (ppm): 2.44 (s, 3H, CH_3), 6.19 (s, 4H, $2NH_2$, D_2O-exchangeable), 7.51 (d, 2H, $H_{3,5}$, 4-Cl–C_6H_4, J = 8.1 Hz), 7.69 (d, 2H, $H_{2,6}$, 4-Cl–C_6H_4, J = 8.1 Hz), 7.89 (d, 2H, Ph-$H_{3,5}$, J = 7.5 Hz), 7.95 (d, 2H, Ph-$H_{2,6}$, J = 7.5 Hz), 8.52 (s, 1H, –CH═N), and 10.80 (s, 1H, NH, D_2O-exchangeable); ^{13}C NMR (100 MHz, DMSO-d_6) δ (ppm): 14.60, 115.19, 120.11, 120.25, 127.45, 128.84, 129.06, 129.64, 133.33, 134.96, 135.36, 154.97, 156.37, 158.34, 163.81, and 187.57; MS [*m*/*z*, %]: 380 [M^+, 1.63]; Anal. calcd. for $C_{18}H_{17}ClN_8$ (%): C, 56.77; H, 4.50; N, 29.42. Found: C, 56.94; H, 4.57; N, 29.60.

*1-{4-[(3-Amino-5-{[1-(4-chlorophenyl)ethylidene]amino}-1H-pyrazol-4-yl)diazenyl]phenyl}ethanone (**8b**)*

M.p. 213–215°C; yield 60%; IR (KBr, cm^{-1}): 3,394, 3,299, 3,190 (NH, NH_2), 1,662 (C═O), 1,613 (C═N), and 1,561 (N═N); ^{1}H NMR (300 MHz, DMSO-d_6) δ (ppm): 2.02 (s, 3H, N═C–CH_3), 2.56 (s, 3H, CH_3), 6.34 (s, 2H, NH_2, D_2O-exchangeable), 7.50–7.64 (m, 4H, Ar-H), 7.70 (d, 2H, Ph-$H_{3,5}$, J = 8.4 Hz), and 7.92 (d, 2H, Ph-$H_{2,6}$, J = 8.4 Hz); ^{13}C NMR (100 MHz, DMSO-d_6) δ (ppm): 15.15, 27.08, 114.82, 120.57, 120.70, 125.54, 127.66, 128.72, 128.91, 129.73, 134.44, 134.90, 135.81, 138.36, 142.34, 152.92, 158.31, and 197.36; MS [*m*/*z*, %]: 380 [M^+, 6.18]; Anal. calcd. for $C_{19}H_{17}ClN_6O$ (%): C, 59.92; H, 4.50; N, 22.07. Found: C, 60.04; H, 4.57; N, 22.19.

*{4-[1-(Hydrazonoethyl)phenyl]diazenyl}(4-methylbenzylidene)-1H-pyrazole-3,5-diamine (**8c**)*

M.p. 218–220°C; yield 54%; IR (KBr, cm^{-1}): 3,397, 3,280, 3,178 (NH, NH_2), 1,605 (C═N), and 1,559 (N═N); ^{1}H NMR (300 MHz, DMSO-d_6) δ (ppm): 2.37 (s, 3H, tolyl-H), 2.40 (s, 3H, CH_3), 5.99 (s, 2H, NH_2, D_2O-exchangeable), 7.29 (d, 2H, $H_{3,5}$ 4-CH_3–C_6H_4, J = 7.8 Hz), 7.70 (d, 2H, Ph-$H_{3,5}$, J = 8.4 Hz), 7.76 (d, 2H, $H_{2,6}$, 4-CH_3–C_6H_4, J = 7.8 Hz), 7.94 (d, 2H, Ph-$H_{2,6}$, J = 8.4 Hz), and 8.48 (1H, CH═ N); ^{13}C NMR (100 MHz, DMSO-d_6) δ (ppm): 21.59, 25.81, 115.97, 120.52, 127.86, 128.59, 128.63, 129.08, 129.91, 129.99, 132.29, 135.28, 141.31, 152.60, 155.58, 158.18, 163.93, and 175.54; MS [*m*/*z*, %]: 360 [M^+, 18.14]; Anal. calcd. for $C_{19}H_{20}N_8$ (%): C, 63.32; H, 5.59; N, 31.09. Found: C, 63.46; H, 5.65; N, 31.31.

*4-{[4-(1-Hydrazonoethyl)phenyl]diazenyl}(1-p-tolylethylidene)-1H-pyrazole-3,5-diamine (**8d**)*

M.p. 207–210°C; yield 54%; IR (KBr, cm^{-1}): 3,393, 3,296, 3,172 (NH, NH_2), 1,614 (C═N), and 1,557 (N═N); ^{1}H NMR (300 MHz, DMSO-d_6) δ (ppm): 1.63 (s, 3H, N═C–CH_3), 2.03 (s, 3H, tolyl-H), 2.49 (s, 3H, CH_3), 6.32 (s, 2H, NH_2, D_2O-exchangeable), 7.56–7.71 (m, 6H, Ph-$H_{2,6}$, $H_{3,5}$ and $H_{2,6}$, 4-CH_3–C_6H_4), and 7.92 (d, 2H, Ph-$H_{2,6}$); ^{13}C NMR (100 MHz, DMSO-d_6) δ (ppm): 21.35, 25.75, 27.05, 114.95, 115.72, 116.81, 120.45, 120.54, 125.54, 126.88, 127.57, 129.44, 129.73, 134.21, 138.16, 142.47, 153.03, 155.18, 157.59, and 175.87; MS [*m*/*z*, %]: 374 [M^+, 0.83]; Anal. calcd. for $C_{20}H_{22}N_8$ (%): C, 64.15; H, 5.92; N, 29.93. Found: C, 64.28; H, 6.01; N, 30.18.

*4-{[4-(1-Hydrazonoethyl)phenyl]diazenyl}(4-methoxybenzylidene)-1H-pyrazole-3,5-diamine (**8e**)*

M.p. 180–183°C; yield 41%; IR (KBr, cm^{-1}): 3,446, 3,292, 3,178 (NH, NH_2), 1,637 (C═N), and 1,595 (N═N); ^{1}H NMR (300 MHz, DMSO-d_6) δ (ppm): 2.42 (s, 3H, CH_3), 3.83 (s, 3H, OCH_3), 7.68–8.01 (m, 8H, Ar-H), 8.48 (s, 1H, CH═N), and 12.24 (s, 1H, NH, D_2O-exchangeable) ppm; ^{13}C NMR (100 MHz, DMSO-d_6) δ (ppm): 25.76, 55.90, 82.47, 114.84, 120.38, 126.80, 128.90, 129.73, 130.93, 131.12, 152.60, 157.66, 162.90, 168.80, and 175.55; MS [*m*/*z*, %]: 376 [M^+, 1.68];

Anal. calcd. for $C_{19}H_{20}N_8O$ (%): C, 60.63; H, 5.36; N, 29.77. Found: C, 60.79; H, 5.44; N, 29.92.

*1-{4-[(3-Amino-5-{[1-(4-methoxyphenyl)ethylidene]amino}-1H-pyrazol-4-yl)diazenyl]phenyl}ethanone (**8f**)*

M.p. 199–201°C; yield 45%; IR (KBr, cm^{-1}): 3,388, 3,293, 3,174 (NH, NH_2), 1,663 (C═O), 1,612 (C═N), and 1,558 (N═N); ^{1}H NMR (300 MHz, DMSO-d_6) δ (ppm): 2.03 (s, 3H, N═C–CH_3), 2.56 (s, 3H, CH_3), 3.83 (s, 3H, OCH_3), 6.34 (s, 2H, NH_2, D_2O-exchangeable), 7.62–7.96 (m, 8H, Ar-H), and 10.89 (s, 1H, NH, D_2O-exchangeable); ^{13}C NMR (100 MHz, DMSO-d_6) δ (ppm): 15.01, 27.06, 55.71, 114.21, 114.27, 114.89, 116.69, 120.50, 120.58, 125.54, 127.59, 128.49, 129.73, 134.31, 138.25, 142.39, 152.98, 157.51, 175.69, and 197.34; MS [*m/z*, %]: 376 [M^+, 1.90]; Anal. calcd. for $C_{20}H_{20}N_6O_2$ (%): C, 63.82; H, 5.36; N, 22.33. Found: C, 63.97; H, 5.42; N, 22.52.

*4-[({3-Amino-4-[4-(1-hydrazonoethyl)phenyl]diazenyl}-1H-pyrazol-5-yl)imino]methyl}phenol (**8g**)*

M.p. 278–280°C; yield 62%; IR (KBr, cm^{-1}): 3,441–3,156 (OH, NH, NH_2), 1,608 (C═N), and 1,554 (N═N); ^{1}H NMR (300 MHz, DMSO-d_6) δ (ppm): 2.45 (s, 3H, CH_3), 6.00 (s, 2H, NH_2, D_2O-exchangeable), 6.60 (s, H, OH, D_2O-exchangeable), 6.79 (d, 2H, $H_{3,5}$, 4-OH–C_6H_4), 7.62–7.71 (m, 4H, Ph-$H_{2,6}$ and $H_{2,6}$, 4-OH–C_6H_4), 7.91 (d, 2H, Ph-$H_{3,5}$), and 8.40 (1H, CH═N); ^{13}C NMR (100 MHz, DMSO-d_6) δ (ppm): 25.71, 87.60, 115.85, 116.72, 120.50, 127.66, 130.54, 135.69, 145.50, 155.32, 159.01, 162.92, 175.26; MS [*m/z*, %]: 362 [M^+, 28.94]; Anal. calcd. for $C_{18}H_{18}N_8O$ (%): C, 59.66; H, 5.01; N, 30.92. Found: C, 59.81; H, 5.09; N, 31.13.

*4-[1-({3-Amino-4-[4-(1-hydrazonoethyl)phenyl]diazenyl}-1H-pyrazol-5-yl)imino]ethyl}phenol (**8h**)*

M.p. 215–218°C; yield 58%; IR (KBr, cm^{-1}): 3,393–3,187 (OH, NH, NH_2), 1,612 (C═N), and 1,559 (N═N); ^{1}H NMR (300 MHz, DMSO-d_6) δ (ppm): 1.66 (s, 3H, N═C–CH_3), 2.43 (s, 3H, CH_3), 6.00 (s, H, OH, D_2O-exchangeable), 6.35 (s, 2H, NH_2, D_2O-exchangeable), 6.81 (d, 2H, $H_{3,5}$, 4-OH–C_6H_4), 7.58–7.91 (m, 4H, Ph-H_2,6 and $H_{2,6}$, 4-OH–C_6H_4), 7.93 (d, 2H, Ph-$H_{3,5}$), and 11.00 (s, 1H, NH, D_2O-exchangeable); ^{13}C NMR (100 MHz, DMSO-d_6) δ (ppm): 14.56, 25.38, 114.50, 116.38, 120.01, 125.03, 126.31, 126.51, 127.06, 129.21, 133.66, 135.26, 137.62, 141.95, 152.56, 154.71, 157.13, and 175.21; MS [*m/z*, %]: 376 [M^+, 3.13]; Anal. calcd. for $C_{19}H_{20}N_8O$ (%): C, 60.63; H, 5.36; N, 29.77. Found: C, 60.79; H, 5.41; N, 29.89.

4.2 | In vitro antitumor assay

4.2.1 | Methodology: cell culture

Cancer cells from the breast cancer cell line (MCF-7, human breast adenocarcinoma) were purchased from American Type Cell Culture Collection (Manassas) and grown in an appropriate growth medium, Dulbecco's modified Eagle's medium (DMEM) or Roswell Park Memorial Institute (RPMI)-1640 medium, supplemented with 100 mg/ml of streptomycin, 100 units/ml of penicillin, and 10% of heat-inactivated fetal bovine serum, in a humidified 5% (v/v) CO_2 atmosphere at 37°C.

4.2.2 | Cell growth inhibitory assay

Cytotoxicity was determined using the MTT method. Exponentially growing cells from the MCF-7 cancer cell line were trypsinized, counted, and seeded at the appropriate densities (2,000–1,000 cells/0.33 cm^2 well) in 96-well microtiter plates. Cells then were incubated in a humidified atmosphere at 37°C for 24 hr. Then, cells were exposed to different concentrations of compounds (0.1, 10, 100, and 1,000 μM) for 72 hr. Then the viability of treated cells was determined using MTT technique as follows: Media were removed, cells were incubated with 200 μl of 5% MTT solution/well (Sigma-Aldrich, MO), and they were allowed to metabolize the dye into colored insoluble formazan crystals for 2 hr. The remaining MTT solution was discarded from the wells and the formazan crystals were dissolved in 200 μl/well of acidified isopropanol for 30 min, covered with aluminum foil, and with continuous shaking using a MaxQ 2000 plate shaker (Thermo Fisher Scientific Inc., MI) at room temperature. Absorbance was measured at 570 nm using a Stat FaxR 4200 plate reader (Awareness Technology, Inc., FL). The cell viability was expressed as a percentage of control and the concentration that induces 50% of maximum inhibition of cell proliferation (IC_{50}) was determined using GraphPad Prism version 5 software (GraphPad Software Inc., CA).[43,44]

4.2.3 | Cell cycle analysis (DNA flow cytometry analysis)

MCF-7 cells at a density of 4×10^6 cells/T-75 flask were exposed to **8b** at its IC_{50} concentration for 24 hr. The cells then were collected by trypsinization, washed in phosphate-buffered saline (PBS), and fixed in ice-cold absolute alcohol. Thereafter, cells were stained using Cycle TEST™ PLUS DNA Reagent Kit (BD Biosciences, San Jose, CA) according to the manufacturer's instructions. Cell cycle distribution was established using a FACSCalibur flow cytometer (BD Biosciences).

4.2.4 | Annexin V-FITC assay

MCF-7 cells were seeded in a six-well plate (1×10^5 cells/well), incubated for 24 hr, and then treated with vehicle (0.1% DMSO) or 3.08 μM of compound **8b** for 24 hr. The cells were then harvested, washed using PBS, stained for 15 min at room temperature in the dark using annexin V-FITC and PI in binding buffer (10mM 4-(2-hydroxyethyl)-1-piperazineethanesulfonic acid, 140 mM NaCl, and 2.5 mM $CaCl_2$ at pH 7.4), and then analyzed by the flow cytometer.[45]

4.2.5 | Determination of CDK2/cyclin E kinase activity

The effect of **8b** on the activity of CDK2/cyclin E kinase was measured using serine/threonine-protein kinase CDK2/Cyclin E, ADP-Glo Kinase assay (catalog #v4488). The cells were centrifuged for 15 min at 1,000*g*, 2–8°C, and assayed immediately according to the manufacturer's instructions. Shortly, the assay was performed using 100 ml of supernatant in cells in each well, which were incubated for 2 hr at 37°C before starting the assay procedure. Finally, the luminescence was recorded (Integration time 0.5–1 s).

ACKNOWLEDGMENTS

The authors are grateful to all members of the cell culture lab, College of Pharmacy, Al-Azhar University, for carrying out the antitumor activity and to confirmatory diagnostic unit VACSERA-EGYPT for carrying out the CDK2 assay.

CONFLICTS OF INTERESTS

The authors declare that there are no conflicts of interests.

ORCID

Amel M. Farrag http://orcid.org/0000-0002-8207-0859

REFERENCES

[1] Cancer, https://www.who.int/en/news-room/fact-sheets/detail/cancer. Accessed June 14, 2020.
[2] L. A. Torre, F. Bray, R. L. Siegel, J. Ferlay, J. Lortet-Tieulent, A. Jemal, *CA Cancer J. Clin.* **2015**, *65*, 87.
[3] Cancer Statistics—National Cancer Institute, https://www.cancer.gov/about-cancer/understanding/statistics. Accessed June 15, 2020.
[4] U.S. Breast Cancer Statistics | Breastcancer.org, https://www.breastcancer.org/symptoms/understand_bc/statistics. Accessed June 16, 2020.
[5] M. T. Park, S. J. Lee, *J. Biochem. Mol. Biol.* **2003**, *36*, 60.
[6] G. Küçükgüzel, S. Şenkardeş, *Eur. J. Med. Chem.* **2015**, *97*, 786.
[7] J. Bronson, M. Dhar, W. Ewing, N. Lonberg, *Annual Reports in Medicinal Chemistry*, Academic Press Inc., Amsterdam, the Netherlands **2012**, pp. 499–569.
[8] P. J. Roberts, *Biol. Targets Ther.* **2013**, *7*, 91.
[9] V. Kryštof, P. Cankař, I. Fryšová, J. Slouka, G. Kontopidis, P. Džubák, M. Hajdúch, J. Srovnal, W. F. de Azevedo, M. Orság, M. Paprskářová, J. Rolčík, A. Látr, P. M. Fischer, M. Strnad, *J. Med. Chem.* **2006**, *49*, 6500.
[10] R. Jorda, E. Schütznerová, P. Cankař, V. Brychtová, J. Navrátilová, V. Kryštof, *Bioorg. Med. Chem.* **2015**, *23*, 1975.
[11] A. M. Fouda, H.-A. S. Abbas, E. H. Ahmed, A. A. Shati, M. Y. Alfaifi, S. E. I. Elbehairi, *Molecules* **2019**, *24*, 1080.
[12] M. M. F. Ismail, D. H. Soliman, A. M. Farrag, R. Sabour, *Int. J. Pharm. Pharm. Sci.* **2016**, *8*, 2625.
[13] A. S. Girgis, J. Stawinski, N. S. M. Ismail, H. Farag, *Eur. J. Med. Chem.* **2012**, *47*, 312.
[14] M. A. Abdelgawad, K. R. A. Abdellatif, O. M. Ahmed, *Med. Chem.* **2014**, *231*, 1.
[15] N. M. Saleh, Y. A. Ammar, J. A. Micky, H. A. S. Abbas, M. S. A. El-Gaby, *Indian J. Chem.—Sect. B, Org. Med. Chem.* **2004**, *43*, 2195.
[16] P. C. Tsai, I. J. Wang, *Dyes Pigments* **2007**, *74*, 578.
[17] A. El-Shafei, A. A. Fadda, A. M. Khalil, T. A. E. Ameen, F. A. Badria, *Bioorg. Med. Chem.* **2009**, *17*, 5096.
[18] P. D. Kale, *J. Chem. Pharm. Res.* **2013**, *5*, 130.
[19] S. H. Mashraqui, L. S. Jadhav, *Indian J. Chem.* **2004**, *43B*, 927.
[20] H. a K. Salih, I. K. Jassim, S. Abdalsatar, *J. Al-Nahrain Univ. Sci.* **2007**, *10*, 18.
[21] J. M. Lee, M. S. Lee, D. Koh, Y. H. Lee, Y. Lim, S. Y. Shin, *Cancer Lett.* **2014**, *354*, 348.
[22] H. A. M. Andree, C. P. M. Reutelingsperger, R. Hauptmann, H. Coenraad Hemker, W. Th. Hermen, G. M. Willems, *J. Biol. Chem* **1990**, *265*, 4923.
[23] I. Vermes, C. Haanen, H. Steffens-Nakken, C. Reutelingsperger, *J. Immunol. Methods* **1995**, *184*, 39.
[24] D. B. Farag, N. A. Farag, A. Esmat, S. A. Abuelezz, E. Abdel-Salam Ibrahim, D. A. Abou El Ella, *MedChemComm* **2015**, *6*, 283.
[25] W. M. Eldehna, A. Altoukhy, H. Mahrous, H. A. Abdel-Aziz, *Eur. J. Med. Chem.* **2015**, *90*, 684.
[26] M. A. Salem, M. S. Behalo, E. Elrazaz, *Med. Chem. Res.* **2019**, *28*, 1223.
[27] A. Daina, O. Michielin, V. Zoete, *Sci. Rep.* **2017**, *7*, 1.
[28] Molsoft L.L.C.: Drug-Likeness and molecular property prediction, http://molsoft.com/mprop/. Accessed May 27, 2020.
[29] ADME Prediction—PreADMET | Prediction of ADME/Tox, https://preadmet.bmdrc.kr/adme-prediction/. Accessed May 27, 2020.
[30] http://www.openmolecules.org/datawarrior/. Accessed May 27, 2020.
[31] M. Orita, K. Ohno, M. Warizaya, Y. Amano, T. Niimi, *Methods Enzymol.*, Elsevier, **2011**, pp. 383–419.
[32] G. M. Keserü, G. M. Makara, *Nat. Rev. Drug Discov.* **2009**, *8*, 203.
[33] Y. H. Zhao, M. H. Abraham, J. Le, A. Hersey, C. N. Luscombe, G. Beck, B. Sherborne, I. Cooper, *Pharm. Res.* **2002**, *19*, 1446.
[34] H. S. A. El-Zahabi, M. M. A. Khalifa, Y. M. H. Gado, A. M. Farrag, M. M. Elaasser, N. A. Safwat, R. R. Abdel Raouf, R. K. Arafa, *Eur. J. Pharm. Sci.* **2019**, *130*, 124.
[35] S. J. Capuzzi, E. N. Muratov, A. Tropsha, *J. Chem. Inf. Model.* **2017**, *57*, 417.
[36] R. Thangavelu, M. Sai Harika, T. Raj Kumar, L. Siva Sankar Reddy, *Int. J. Pharm. Sci. Res.* **2017**, *8*, 1677.
[37] Á. Tarcsay, K. Nyíri, G. M. Keserú, *J. Med. Chem.* **2012**, *55*, 1252.
[38] C. W. Murray, D. A. Erlanson, A. L. Hopkins, G. M. Keserü, P. D. Leeson, D. C. Rees, C. H. Reynolds, N. J. Richmond, *ACS Med. Chem. Lett.* **2014**, *5*, 616.
[39] H. Chen, O. Engkvist, T. Kogej, *The Practice of Medicinal Chemistry*, Elsevier, London **2015**, pp. 379–393.
[40] I. Jabeen, K. Pleban, U. Rinner, P. Chiba, G. F. Ecker, *J. Med. Chem.* **2012**, *55*, 3261.
[41] A. G. Al-Sehemi, A. Irfan, A. M. Fouda, *Spectrochim. Acta Part A, Mol. Biomol. Spectrosc.* **2013**, *111*, 223.
[42] K. T. Mahmudov, A. M. Maharramov, R. A. Aliyeva, I. A. Aliyev, R. K. Askerov, R. Batmaz, M. N. Kopylovich, A. J. L. Pombeiro, *J. Photochem. Photobiol. A Chem.* **2011**, *219*, 159.
[43] T. Mosmann, *J. Immunol. Methods* **1983**, *65*, 55.
[44] D. A. Scudiere, R. H. Shoemaker, K. D. Paul, A. Monks, S. Tierney, T. H. Nofziger, M. J. Currens, D. Seniff, M. R. Boyd, *Cancer Res.* **1988**, *48*, 4827.
[45] K. K. W. Lo, T. K. M. Lee, J. S. Y. Lau, W. L. Poon, S. H. Cheng, *Inorg. Chem.* **2008**, *47*, 200.

SUPPORTING INFORMATION

Additional supporting information may be found online in the Supporting Information section.

How to cite this article: Ismail MMF, Soliman DH, Sabour R, Farrag AM. Synthesis of new arylazopyrazoles as apoptosis inducers: Candidates to inhibit proliferation of MCF-7 cells. *Arch Pharm*. 2020;e2000214.
https://doi.org/10.1002/ardp.202000214